15th Australasian Fluid Mechanics Conference
The University of Sydney, Sydney, Australia
13-17 December 2004

Mean Flow Characteristics of a Micro-injector Induced Swirling Jet

I. K. Toh, P. O'Neill, D. Honnery and J. Soria

Laboratory for Turbulence Research in Aerospace & Combustion
Department of Mechanical Engineering
Monash University, Melbourne, Victoria 3800, AUSTRALIA

Abstract

A novel method of generating a swirling jet using micro-injectors to introduce the required tangential component into an axial jet has been developed. This method allows the flow rate of the axial jet and the tangential micro-injectors to be varied independently. Thus the controlling parameters, Reynolds number (*Re*) and swirl number (*S*), can be varied precisely. This level of control enables detailed investigation of the phenomena associated with swirling jets.

Introduction

The large scale effects of swirl in fluid flow have been appreciated for many decades. It affects the jet growth, entrainment and decay of non-reacting jets, and flame size, shape and stability of combusting jets. There are a number of ways of generating a swirling jet; namely axial plus tangential entry, guided vanes and direct rotation. Chigier and Chervinsky [1] have carried out experiments using an axial plus tangential entry swirl generator. They were able to generate jets with no swirl to strongly swirling with reverse flow. Gore and Ranz [2] imparted rotation to axial pipe flow by means of a rotating perforated plate in which holes were drilled either parallel to the axis or at 45° to the axis. They found that the flow generated was not axisymmetric and the flow field was complicated by additional secondary flow induced by the vanes. Rose [3], on the other hand, rotated a pipe of 100 diameters in length at 9500 RPM to generated a fully develop swirling jet. The swirl motion is generated solely by the friction force between the air and the inner wall of the pipe. Due to the relatively low viscosity of the air, Rose was only able to generate relatively weak swirl.

In the experiment conducted here, a swirl velocity component is induced in an axial jet by micro-injectors. The combined flow is then discharged through an orifice. This method allows for independent and precise control of the resulting flow and its structure. In the present study, jets with different Reynolds numbers (*Re*) and swirl numbers (*S*), which define the characteristics of the flow, are investigated using particle image velocimetry (PIV).

Experimental Methods

In this experimental study, velocity field measurements were taken in a jet with micro-injector induced swirl. Figure 1 shows the coordinate system used. Figure 2 shows the micro-jet swirl generator and the experimental apparatus. The air supply to the main jet was separate from the micro-jets supply. This allowed the flow rate of the axial jet and the micro-jets to be varied independently. To enable PIV measurements, the main axial jet supply was seeded with olive oil droplets around 1μm in diameter. The unseeded micro-jets supply was directed into the reservoir, figure 2, before it was injected tangentially into the settling chamber through eight 0.5×0.5mm square cross section micro-injectors. The combined flow then passed through a contraction with an area ratio of 25, thence through an 8mm diameter orifice at the exit of the nozzle. The nozzle was mounted in a vertical wind tunnel, figure 2. This set up permits investigation of the effect of co-flow on the swirling jet. In the present study, no co-flow was used.

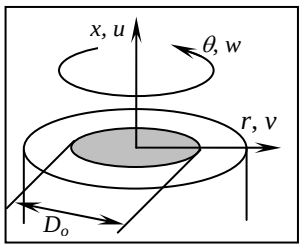

Figure 1: Coordinate system.

A Quanta system dual Nd:YAG laser with the wavelength of 532nm was used to illuminate the seeding particles. The laser is capable of producing two 200mJ pulses of 6 ns duration at a repetition rate of up to 10Hz. System timing was controlled by a computer running Real Time Linux. Time intervals between each laser pulse ranged from 7-40μs depending on the experiment.

The images required for PIV analysis were acquired using a PCO Sensicam 12bit cooled digital camera that operates in a double shutter mode. Images obtained from the camera were stored in the image acquisition computer. Images in the both the vertical *(x-r)* and azimuth plane *(r-θ)* were acquired. Orientation of the camera was such that a CCD array of 1280×1024pixels was used for images in vertical plane, while CCD array of 1024×1024pixels was used for images in azimuth plane. A 105mm Nikkor lens was used for images acquired in the vertical plane, while a 200mm Micro-Nikkor lens was used in the azimuth plane.

Figure 2 shows the configuration where the images in the azimuth plane were acquired. A high reflective mirror at 45° was placed above the nozzle to direct the light from the seed particles illuminated by the horizontal laser sheet. For acquiring images in the vertical plane, the mirror was removed and laser sheet rotated by 90° along the axis of the aperture.

The image pairs were analysed using the Multi-grid Cross Correlation Digital Particle Image Velocimetry (MCCDPIV) algorithm described in Soria et al [4], which has its origin in an iterative and adaptive cross-correlation algorithm introduced by Soria [5] and [6]. Details of the performance, accuracy and uncertainty of the MCCDPIV algorithm with applications to the analysis of a single exposed PIV and holographic PIV (HPIV) images have been reported in [7] and [8].

The present single exposed image acquisition experiments were designed for a two-pass MCCDPIV analysis. The first pass used typically an interrogation window IW = 32 pixels, while the second pass used an IW = 24 pixels with discrete IW offset to minimize the measurement uncertainty [9]. The sampling spacing between the centres of the IW was 24 pixels. The MCCDPIV

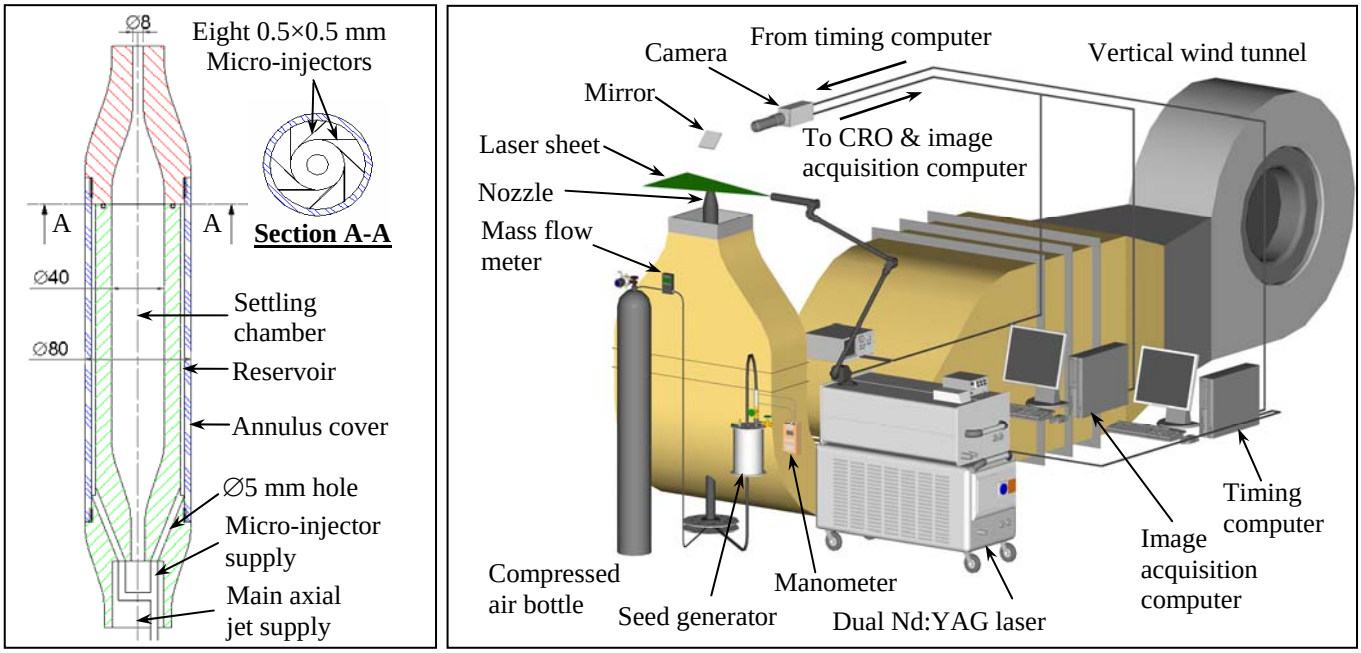

Figure 2: Drawing of nozzle design (left) and schematic diagram of experimental apparatus (right).

algorithm incorporates the local cross-correlation function multiplication method introduced by [10] to improve the search for the location of the maximum value of the cross-correlation function. For the sub-pixel peak calculation, a two dimensional Gaussian function model was used to find, in a least square sense, the location of the maximum of the cross-correlation function [5]. The MCCDPIV data field was subsequently validated by applying: (i) a global histogram operator check [11], (ii) a median test [12], and (iii) the dynamic mean value operator test described in [12]. The tests were applied in the specified order. Following data validation, the in-plane velocity components *(u,v)* in the *(x,r)* coordinate directions respectively were computed by dividing the measured MCCDPIV displacement in each interrogation window by the time between the exposures of the image pair. The uncertainty relative to the maximum velocity in the velocity components at the 95% confidence level for these measurements is 0.3%.

Results

Two non-dimensional numbers can characterize a swirling jet: the Reynolds number and the swirl number. The Reynolds number used is based on the average axial velocity (U_o) at the orifice and the orifice diameter (D_o),

$$Re = \frac{\rho U_o D_o}{\mu} \quad . \tag{1}$$

The swirl number is normally defined as the axial flux of swirl momentum divided by the axial flux of axial momentum times the equivalent nozzle radius [13]:

$$S = \frac{G_\theta}{G_x D_o / 2} \quad . \tag{2}$$

This characterization is often very difficult to measure with certainty. Thus, simplification of the equation is necessary. One common assumption made is to treat the flow as a solid body rotation plug flow at the nozzle. The turbulent stress term is also often neglected [13]. The swirl number can then be simplified to,

$$S = \frac{G/2}{1-(G/2)^2}, \tag{3}$$

where G is the ratio of the maximum tangential velocity to maximum axial velocity measured at the nozzle. This equation is valid up to a swirl number of about $S \approx 0.2$ [13].

Figure 3 shows the radial distribution of the normalised mean axial velocity for a set of four experimental conditions. The corresponding non-dimensionalised tangential velocity profiles are shown in figure 4. PIV data processing parameters are listed in table 1 and 2 respectively. In this experiment, The Reynolds number was kept at a fairly constant level, (ranges from 3773 to 3982) while the swirl number was varied progressively.

In figure 3, axial velocity (u) is normalised by the local maximum velocity (u_m). The radial position r is normalised by $(x+a)$, where a is the apparent distance of the origin of the jet from the orifice. According to Chigier and Chervinsky [1], the apparent distance of the jet's origin from the orifice can be obtained by extrapolating the line of the reciprocal of centre line axial velocity, $1/u_m$ against x. The value of a is given by the value of x at $1/u_m = 0$. The linear function was fitted to the data points at the far field (self similarity region) in order to obtain a more accurate a value. Only the data points where $x > 4D_o$ were used for the linear extrapolation.

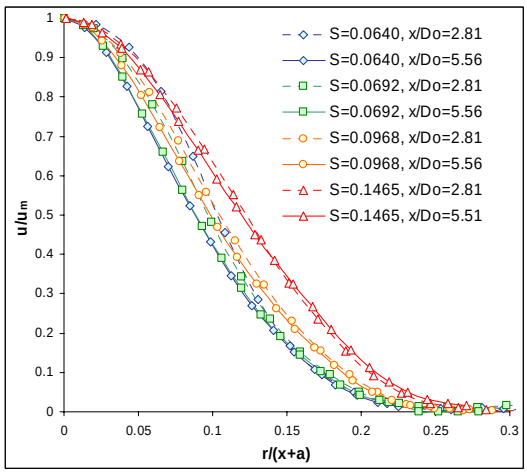

Figure 3: Radial distributions of normalised axial velocity (constant *Re*, varying *S*).

The velocity profiles shown in figure 3 exhibit typical Gaussian profiles, which is consistent with previous results for weakly swirling jets [1]. The increased spread of the jet when swirl intensity is increased is clearly evident in figure 3. The velocity profiles exhibit self similarity within the experimental region.

This agrees well with the results of Chigier and Chervinsky (1967) [1], who observed self similarity within 4 diameters of the orifice of weakly swirling jets.

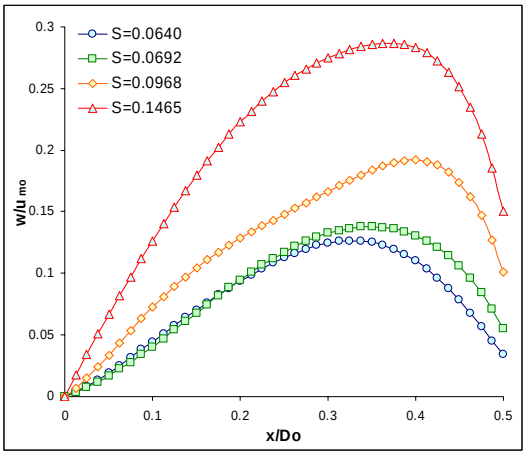

Figure 4: Radial distribution of mean tangential velocity (constant *Re*, varying *S*).

Figure 4 shows the radial distribution of integrated mean tangential velocity of the swirling jets. The tangential velocity profiles plotted are in the *r*-θ plane. The tangential velocity is normalised by the maximum axial velocity. The magnitude of the tangential velocity of the jet with higher swirl number is obviously higher and it peaks at a normalised radius closer to the edge of the jet. The inner region of the profile is almost linear and corresponds to solid body rotation plug flow.

Position	$0D_o$ - $5.8D_o$
Image area	46.7 × 37.4mm^2 $5.8D_o$ × $4.7D_o$
CCD array	1280 × 1024pixel^2
Spatial resolution	27.4pixels/mm 219.2pixels/Do
Number of image pairs	1120
Vectors spacing	24pixels
First interrogation window size	32 × 32pixels^2
Second interrogation window size	24 × 24pixels^2

Table 1: MCCDPIV parameters (x – r plane).

Position	0.47mm $0.06D_o$ above the nozzle
Image area	8.7 × 8.7mm^2 $1.09D_o$ × $1.09D_o$
CCD array	1024 × 1024pixel^2
Spatial resolution	118.3pixels/mm 946pixels/D_o
Number of image pairs	1100
Vectors spacing	24pixels
First interrogation window size	32 × 32pixels^2
Second interrogation window size	24 × 24pixels^2

Table 2: MCCDPIV parameters (r – θ plane).

Figure 5 shows the radial distribution of the normalised mean axial velocity for a different set of four experimental conditions. The corresponding non-dimensionalised tangential velocity profile is shown in figure 6. The PIV data processing parameters are similar to those listed in table 1 and 2. The swirl number is fixed in the range of 0.0631 to 0.0648 while the Reynolds number is varied progressively.

The decrease in jet width as Reynolds number increases is clearly shown in figure 6. The effect of Reynolds number is counteracting the effect due to the increase in swirl intensity.

Figure 6 shows that swirling jets with different Reynolds number exhibit similar normalised tangential velocity profile. Increase in Reynolds number shifts the location of maximum tangential velocity towards the edge of the jet.

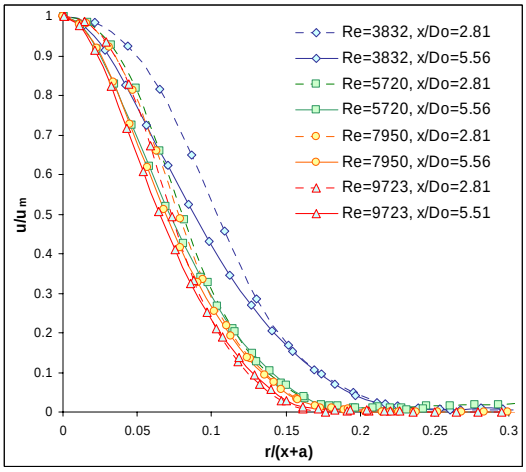

Figure 5: Radial distributions of normalised axial velocity (constant *S*, vary *Re*).

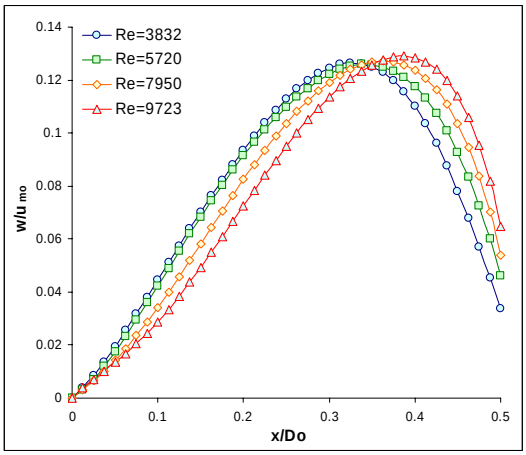

Figure 6: Radial distribution of mean tangential velocity (Constant *S*, vary *Re*).

Velocity profile in the self similar region can be approximated using Gaussian curve according to the following equation [1]

$$u / u_m = exp(-k_u \xi), \qquad (4)$$

where $\xi = r/(x+a)$,
k_u = Gaussian velocity error curve constant.

k_u is determined from the measured value of ξ and u/u_m when u/u_m = 0.5. The experimental determined k_u is plotted against swirl number in figure 7. In the region of swirl number investigated, k_u decreases almost linearly with *S*. The data collected in this study is consistence with previous literature [1].

The angle of spread, α is defined as [14]

$$\alpha = tan^{-1}\left(\frac{r_{1/2}}{(x+a)}\right). \qquad (5)$$

where $r_{1/2}$ is the radial coordinate where u/u_m = 0.5. The angle of spread obtained in the experiment is graphed in figure 8. Figure 8 shows that as swirl number increases, the angle of spread increases. Thus, the jet width increases. Angle of spread obtained from this study agrees well with previous literature [1] and [3].

The amount of fluid entrained from the surrounding is given by m-m_o and an entrainment constant can be defined such that

$$K_e = \left(\frac{m}{m_o}\right)\left(\frac{D_o}{x}\right). \quad (6)$$

The entrainment constants obtained from this study are plotted in figure 9. The amount of surrounding fluids entrained increases as swirl number increases. The entrainment constants determined are higher than the results obtained by [1] and [2].

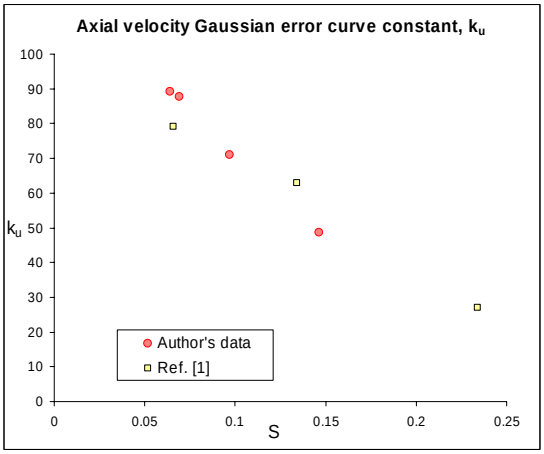

Figure 7: Axial velocity Gaussian error curve constant (k_u) versus S.

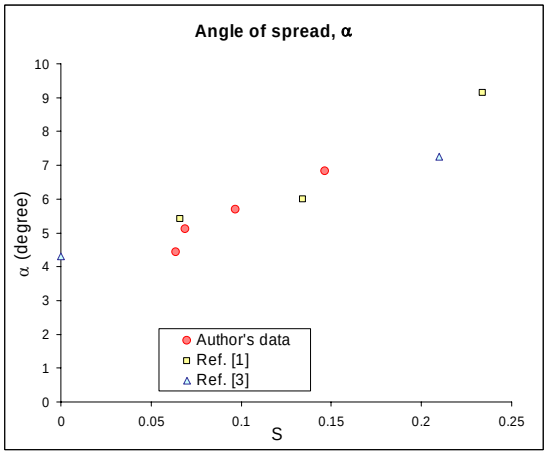

Figure 8: Angle of spread (α) versus S.

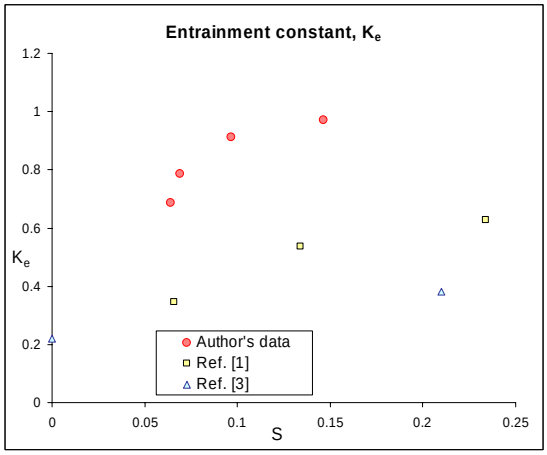

Figure 9: Entrainment constant (K_e) versus S.

Conclusion

A simple method of generating swirling jet with high degree of control of the governing parameters is developed. The experimental investigation conducted covers a range of weak swirling jets. The characteristics of the swirling jets produced are similar to those of previous studies. Empirical constants that describe the swirling jet have been determined. These constants are Gaussian velocity curve constant, angle of spread and entrainment constant. Further investigation is required to determine behaviour of a swirling jet, particularly those with higher degree of swirl.

Acknowledgement

The authors are grateful for the financial support provided by the Monash Research Fund to undertake some of this research.

References

[1] Chigier, N. and Chervinsky, A., Experimental Investigation of Swirling Vortex Motion in Jets, *J. Appl. Mech.*, **34**, 1967, 443 – 451.

[2] Gore, R.W. and Ranz, W.E., Back Flows in Rotating Fluids Moving Axially Through Expanding Cross Sections, *A.I.Ch.E. J.*, **10**, 1964, 83 – 88.

[3] Rose W.G., A Swirling Round Turbulent Jet, *J. Appl. Mech.*, **84**, 1962, 615 – 625.

[4] Soria, J., Cater, J. and Kostas, J., High Resolution Multi-grid Cross Correlation Digital PIV Measurements of a Turbulent Starting Jet Using Half-frame-image-shift film Recording, *Optics & Laser Tech.*, **31**, 1999, 3 – 12.

[5] Soria, J., Digital Cross Correlation Particle Image Velocimetry measurements in the near wake of a circular cylinder, *in: Int. Colloquium on Jets, Wakes and Shear Layers*, CSIRO, Melbourne, Australia, 1994, 25.1 – 25.8.

[6] Soria, J., An Adaptive Cross Correlation Digital PIV Technique for Unsteady Flow Investigations, *in: Masri, A., Honnery D.(Eds.), 1st Australia Conference on Laser Diagnostics in Fluid Mechanics and Combustion*, University of Sydney, NSW, Australia, 1996, 29 – 45.

[7] Soria, J. Multi-grid Approach to Cross Correlation Digital PIV and HPIV Analysis, *in: 13th Australasian Fluid Mechanics Conference*, Monash University, Melbourne, 1998, 381 – 384.

[8] Ellenrieder, K.von, Kostas, J. and Soria, J., Measurements of a Wall-bounded, Turbulent, Separated Flow Using HPIV, *J. Turbulence – selected papers from the 8th European Turbulence Conference*, 2001.

[9] Westerweel, J., Dabiri, D., and Gharib, M., The Effect of a Discrete Window Offset on the Accuracy of Cross Correlation Analysis of Digital PIV Recording, *Exp. Fluids*, **23**, 1997, 20 – 28.

[10] Hart, D., The Elimination of Correlation Error in PIV Processing, *in: 9th International Symposium of Applications of Laser Techniques to Fluid Mechanics*, Lisbon, Portugal, 1998, I:13.3.1 – 13.3.8.

[11] Raffel, M., Willert, C., and Kompenhans, J., Particle Image Velocimetry. *A practical guide*, Springer, 1998.

[12] Westerweel, J., Efficient Detection of Spurious Vectors in Particle Image Velocimetery Data, *Exp. Fluids*, **16**, 1994, 236 – 247.

[13] Gupta. D. Lilley and Syred, N., *Swirling Flows*, Abacus Press, 1984, 1 – 3.

[14] Pope, S. B., *Turbulent Flows*, Cambridge University Press, 2000, 97 – 133.